Structural and Functional Roles of Desmin in Mouse Skeletal Muscle during Passive Deformation

Sameer B. Shah,* Jennifer Davis,* Noah Weisleder,† Ioanna Kostavassili,† Andrew D. McCulloch,* Evelyn Ralston,‡ Yassemi Capetanaki,†§ and Richard L. Lieber*

*Departments of Bioengineering and Orthopaedics, Biomedical Sciences Graduate Group, University of California and Veterans Administration Medical Centers, San Diego, California USA; †Department of Cell Biology, Baylor College of Medicine, Houston, Texas USA; ‡National Institutes of Health, Bethesda, Maryland USA; and §Center for Basic Research, Foundation for Biomedical Research, Academy of Athens, Greece and Department of Biology, University of Patras, Greece

ABSTRACT Mechanical interactions between desmin and Z-disks, costameres, and nuclei were measured during passive deformation of single muscle cells. Image processing and continuum kinematics were used to quantify the structural connectivity among these structures. Analysis of both wild-type and desmin-null fibers revealed that the costamere protein talin colocalized with the Z-disk protein α-actinin, even at very high strains and stresses. These data indicate that desmin is not essential for mechanical coupling of the costamere complex and the sarcomere lattice. Within the sarcomere lattice, significant differences in myofibrillar connectivity were revealed between passively deformed wild-type and desmin-null fibers. Connectivity in wild-type fibers was significantly greater compared to desmin-null fibers, demonstrating a significant functional connection between myofibrils that requires desmin. Passive mechanical analysis revealed that desmin may be partially responsible for regulating fiber volume, and consequently, fiber mechanical properties. Kinematic analysis of α-actinin strain fields revealed that knockout fibers transmitted less shear strain compared to wild-type fibers and experienced a slight increase in fiber volume. Finally, linkage of desmin intermediate filaments to muscle nuclei was strongly suggested based on extensive loss of nuclei positioning in the absence of desmin during passive fiber loading.

INTRODUCTION

Actin-myosin complexes, cytoskeletal proteins including titin and α-actinin, and several associated structural and regulatory proteins provide a basis for active and passive load bearing within muscle sarcomeres. Mechanical integration of a muscle cell requires additional cytoskeletal proteins that permit efficient force transmission within a well-connected sarcomere lattice, and between the cytoskeleton and the extracellular matrix. Hypothesized functional roles of such structural proteins are based largely upon inference from the results of localization studies in fixed tissue or biochemical solution assays. These studies are appropriate for the identification of structural proteins and their potential binding partners. However, they suffer from the fact that 1), only a single representation of cellular structure is obtained from each sample, thus increasing statistical variability; 2), real-time changes in subcellular structure in response to an altered mechanical environment are not detectable; and 3), mechanical properties are rarely measured, precluding direct correlation between mechanical connectivity and function.

The filamentous network formed by intermediate filaments, particularly the muscle-specific protein desmin, is ideally suited to mediate connectivity, given its localization around Z-disks in the extramyofibrillar space (Granger and Lazarides, 1979; Richardson et al., 1981; Tokuyasu et al., 1983; Wang and Ramirez-Mitchell, 1983), near the periodic, dense sarcolemmal protein complexes known as costameres, around the mitochondria, and at the periphery of cell nuclei (Milner et al., 2000; Pardo et al., 1983b; Tokuyasu et al., 1983). This abundance of intermediate filaments within the muscle fiber indeed suggests a role in skeletal muscle function; however, direct evidence for such a role remains sparse.

The longitudinal intermediate filament connections observed between Z-disks (Wang and Ramirez-Mitchell, 1983) suggests their possible contribution to longitudinal load bearing. Two elegant studies probed the contributions of intermediate filaments to muscle passive tension by measuring passive mechanical properties in psoas fiber segments (Wang et al., 1993) and cardiac myocytes (Granzier and Irving, 1995) that were subjected to a series of protein extractions. The studies suggested that although the skeletal muscle intermediate filament network bore passive loads only at nonphysiological sarcomere lengths (SL) $>\sim 5$ μm, in cardiac muscle cells, intermediate filaments contributed to passive tension even at physiological sarcomere lengths between 1.9 and 2.1 μm. In both studies, however, it is possible that the extraction of the major structural components of sarcomeres induced a change in the orientation and local geometry of the remaining components, yielding an altered response to mechanical loading. In addition, as shown by the careful electron microscopy (EM) work of Wang and Ramirez-Mitchell (see Figs. 4–6 in Wang and Ramirez-Mitchell, 1983), extracted myofibrils still exhibit some pockets of severed filaments or pockets of insufficient or excessive extraction. Because the frequency of these regions of extraction-induced non-

Submitted May 12, 2003, and accepted for publication December 3, 2003.

Address reprint requests to Richard L. Lieber, PhD, Dept. of Orthopaedics (9151), VA Medical Center and UC San Diego, 3350 La Jolla Village Dr., San Diego, CA 92161. Tel.: 858-552-8585 ext. 7016; Fax: 858-552-4381; E-mail: rlieber@ucsd.edu.

0006-3495/04/05/2993/16 $2.00

homogeneity have not (to our knowledge) been quantified, it is unclear whether and how local differences in geometry or material properties affect more global properties.

The creation of the desmin-null mouse provided an excellent model to assess directly the relevance of intermediate filaments to muscle development and function. Preliminary characterizations of muscles from desmin-null mice established that the absence of desmin led to significant defects of muscle phenotype (Li et al., 1997; Milner et al., 1996), especially in those muscles that were chronically active such as the heart, soleus, and diaphragm. These studies were followed by a series of rigorous mechanical experiments on whole muscles and muscle bundles, where a wide range of phenotypic differences in active and passive properties were described secondary to the absence of desmin (Anderson et al., 2001; Boriek et al., 2001; Sam et al., 2000). These studies confirmed that desmin was essential for normal muscle mechanical function. However, they could not provide a mechanistic explanation for the variable mechanical response of wild-type and desmin-null muscles, as they lacked a rigorous assessment of individual functional cytoskeletal connections.

In addition to its apparent structural role during mechanical loading, a well-connected cytoskeleton also provides the means to stabilize the cell membrane and to transmit extracellular mechanical signals into the sarcomere lattice. Further, the predictable loading of intracellular structures (e.g., the cell nuclei or the mitochondria) by these signals may also be envisioned, providing a mechanical stimulus for downstream signaling (Maniotis et al., 1997; Milner et al., 2000). Costameres and dystroglycan complexes have been implicated in coupling the cell membrane to the inside of the cell (e.g., Danowski et al., 1992; review by Sunada and Campbell, 1995). Despite their identification, there is significant debate regarding the composition of each of these complexes and their specific mechanical roles. The interactions of intermediate filaments with organelles are not as well understood, though it has been proposed that desmin, vimentin, and peripherin bind to lamin B of the nuclear karyoskeleton (Georgatos and Blobel, 1987; Georgatos et al., 1987; Djabali et al., 1991; Papamarcaki et al., 1991). The possibility of cellular signaling via a network of desmin-mediated interconnections is attractive; however, a structural basis for such pathways in skeletal muscle also has yet to be defined.

In the current study, we assessed directly the relationship between desmin mediated connections and skeletal muscle cell function. We characterized mechanical interactions between three subcellular structures with which desmin is hypothesized to be associated: costamere complexes (represented by the protein talin), sarcomeric Z-disks (represented by the protein α-actinin), and cell nuclei. Furthermore, we developed image processing algorithms and a continuum kinematics model to quantify structural connectivity among these structures.

METHODS AND MATERIALS

Experimental model and design

Experiments were performed on fibers from two groups of adult mice: wild-type (+/+) 129/Sv (Taconic Farms, Germantown, NY) and desmin-null (*des* −/−) 129/Sv (Milner et al., 1996). Mechanics and imaging experiments were performed on fibers from the fifth toe muscle of the extensor digitorum longus (EDL) in age-matched mice (+/+: $n = 7$; *des* −/−: $n = 6$, aged 10–14 weeks). Use of the EDL allowed the application of loads to cells free from confounding effects of preexisting sarcolemmal degeneration or fibrosis present in chronically activated desmin-null muscles such as the soleus, heart, and diaphragm (Li et al., 1997; Milner et al., 1996). In addition, the homogeneity of fiber type in mouse EDL (Burkholder et al., 1994) prevents a differential functional response secondary to variations in the severity of mitochondrial defects in different fiber types (Milner et al., 2000).

A descriptive analysis of nuclear localization in soleus and plantaris muscle fibers was also performed to gauge the extent of phenotypic response in muscles with varying fiber type. Fibers were prepared from the soleus muscle of mice aged 5 weeks and 6 months and from the plantaris muscle of mice aged 5 weeks. For each age, muscle, and genotype, at least 20 fibers or fiber fragments from three different animals were observed.

All procedures were performed in accordance with the National Institutes of Health Guide for the Use and Care of Laboratory Animals and were approved by the University of California and Department of Veterans Affairs Committees on the Use of Animal Subjects in Research. Each mouse was anesthetized with a cocktail composed of [mg/kg]: ketamine [10] , rompum [5] , and acepromazine [1] . Hindlimbs were transected proximal to the knee and immediately placed for further dissection into a mammalian Ringer's solution composed of [mM]: NaCl [137] , KCl [5] , NaH_2PO_4 [1] , $NaHCO_3$ [24] , $CaCl_2$ [2] , $MgSO_4$ [1] , and glucose [11] with 10 mg/l curare. The mouse was then euthanized by intracardiac injection of sodium pentobarbital.

Dissection of single fiber segments and attachment to mechanical apparatus

Methods have been previously described (Shah and Lieber, 2003). Briefly, EDL muscles were dissected from hindlimbs, bathed in relaxing solution for 60 min and placed in a glycerol-based storage solution for no more than three weeks at −20°C. All solutions were made in the presence of the protease inhibitor leupeptin. Single intact fiber segments were carefully dissected and transferred in relaxing solution to a chamber housed in a custom-made mechanical apparatus. For collagenase experiments, muscles were peeled into several bundles and incubated in 1% (wt/v) type IV collagenase (Worthington Biochemical, Freehold, NJ) for one hour at 4°C, before further dissection of fiber segments. Within the chamber, the segment was firmly secured between a force transducer (Aurora Scientific 405A, Aurora, Ontario, Canada), and a rotational bearing (Newport MT-RS, Irvine, CA) mounted on an inverted laser scanning confocal microscope (Zeiss Axiovert 100M, Thornwood, NY), allowing imaging of interactions between specific fluorescently labeled cellular structures during passive loading. To ensure that the glycerol-mediated skinning of fibers during storage did not impact the fiber cytoskeleton, segments displaying abnormal discoloration, localized swelling, or irregular labeling of sarcolemmal proteins (e.g., talin) were discarded (Shah and Lieber, 2003).

Antibody labeling and microscopy

Primary antibodies specific for the Z-disk protein α-actinin (Sigma A7811, St. Louis, MO) were preconjugated to Alexa-Fluor 488 (Molecular Probes A-10235, Eugene, OR) secondary antibodies. A similar protocol was used to conjugate primary antibodies specific for the costamere protein talin (Santa

Cruz, sc-7534, Santa Cruz, CA) to Alexa-Fluor 594 (Molecular Probes A-10239, Eugene, OR) secondary antibodies. The fiber segment was subject to a series of blocking steps and washes, and was incubated in a DNA-binding nuclear dye (Molecular Probes, TOTO-3, Eugene, OR) (1:2000 dilution in 0.1% bovine serum albumin) or in an antibody-dye solution at 4°C for varying periods of time, depending on desired labeling combination (Table 1 in Shah and Lieber, 2003). Preconjugated antibodies for talin and α-actinin were diluted in 0.1% bovine serum albumin at 50 μl/ml and 2 μl/ml, respectively.

Images were captured using a confocal imaging system (LSM 510, Zeiss) with a 32 $\times$ 0.4 Achroplan objective (number 440851, Zeiss). Samples were excited with an Ar-Kr laser with beam splitters and filter sets appropriate for excitation of AF-488 and AF-594 dyes, and a He-Ne laser appropriate for excitation of TOTO-3 dye. A frame of 512 $\times$ 512 pixels was captured at an electronic zoom (decrease of imaging field size) of 4.0, yielding a pixel spacing of 140 nm. Each row of pixels was scanned twice and averaged, and the pinhole size was set between 0.4 and 0.5 Airy units. These settings permitted maximal resolution laterally and axially for the selected objective.

For nuclear staining of soleus and plantaris muscles, hindlimbs were fixed by immersion for 4 h in 2% p-formaldehyde. Individual muscles were dissected and single fibers prepared by teasing with fine forceps. Fibers were stained for 10 min in Hoechst 33342 (bis-benzimide, Sigma, St. Louis, MO; 5 μg/ml in phosphate buffered saline), rinsed once in phosphate buffered saline, and mounted in a drop of Vectashield (Vector Labs., Burlingame, CA) between a glass slide and a coverslip. Fibers were observed with a 25 $\times$ 0.5 lens on a Leica DMR fluorescence microscope (Leica, Deerfield, IL), and photographed with a Coolsnap digital camera (Photometrics, Tucson, AZ) driven by IPLab (Scanalytics, Fairfax, VA).

Passive mechanical protocol

The fiber segment was brought to its resting length, determined as the knot-to-knot fiber segment length at which passive tension was just measurable above the noise level of the force transducer. The segment was preconditioned by three loading cycles of 25% strain, resulting in a change in resting length of $<$1% from the resting length before preconditioning. The segment was then loaded in increments of 10% of the segment length at a rate of ~0.1–0.3 fiber lengths/s. At each length, after two minutes of stress relaxation, a stack of confocal images with 2.1–2.3-μm slice thickness was captured, and steady-state force (within 5% of final force value) was recorded. During the two minutes of stress relaxation, the confocal stage was manipulated to keep the selected region of the fiber in the imaging field.

Osmotic loading

To assess desmin's role in regulating fiber volume, fibers from wild-type and desmin-null mice were subject to osmotic compression. Fibers were mounted in the mechanics chamber, in relaxing solution, and diameter and resting sarcomere length were recorded. Relaxing solution was replaced with a hyperosmotic solution containing 8% dextran T-500 (Amersham Pharmaceuticals, Piscataway, NJ) in relaxing solution. After 15 min (steady state), the diameter and sarcomere length were recorded, and compared to initial values.

TABLE 1 Ratio of periodicity of talin label to α-actinin label

KO/WT	AC/FFT	Mean ± SE
WT	AC	0.508 ± 0.002
WT	FFT	0.517 ± 0.003
KO	AC	0.508 ± 0.001
KO	FFT	0.513 ± 0.001

Calculation of stress and strain

Fiber cross-sectional area was calculated using an elliptical approximation based on major and minor diameters of the imaged segment. Diameter in the *x-y* direction (focal plane) was measured from a phase image of the fiber at each stretch. Diameter in the axial direction was determined by taking the difference of the focus position on the top and bottom edges of the fiber. Cauchy (true) stress was calculated by dividing force by the current cross-sectional area, and La Grangian stress was calculated by dividing force by the cross-sectional area of the undeformed fiber.

Average sarcomere length for each confocal slice was calculated by applying the autocorrelation function A_F, a special case of the cross-correlation function C_{FG}, to the α-actinin intensity profile for each row across the entire fiber width. The unbiased cross-correlation function at a point i over a window of size $(2W + 1)$ was calculated as:

$$C_{FG}(m) = \frac{\sum_{u=i-w}^{i+w} F(u)\,G(u-m)}{N-m},$$

for $-w \le m \le w$ pixel lags. Note that $G(u) = F(u)$ for the autocorrelation function. Correlation functions generated a peak at pixel lags in phase with the periodicity of the intensity profile. The autocorrelation function also amplified the intensity profile by a power of two at its peaks, resulting in an increased signal/noise ratio compared to the raw intensity profile (Shah and Lieber, 2003). A fast Fourier transform (FFT) was applied to the amplified intensity profile, and sarcomere length was calculated as the reciprocal of the power spectrum peak frequency. Costamere periodicity was calculated by applying these same signal processing techniques to the intensity profiles of the talin label located at the fiber periphery. Sarcomere length was calculated for collagenase experiments using laser diffraction as described previously (Lieber et al., 1984).

Connectivity analysis

Connectivity of Z-disks across the fiber width was defined in terms of the phase shift between adjacent myofibrils across a fiber segment. Beginning at one edge of the fiber, the α-actinin intensity profile of each row was autocorrelated, and cross-correlated with the α-actinin intensity profile at increments of ~0.6 μm across the fiber, approximating the diameter of a myofibril. The phase shift between adjacent myofibrils was calculated as the distance between the auto- and cross-correlation function peaks. Connectivity was expressed as the variance of the mean phase shift across the fiber diameter, with a highly connected lattice showing a low variance. Alternately, calculating the difference in phase shift between consecutive myofibrils and plotting these values as a function of distance across the fiber diameter provided a measure of local connectivity. For this measurement, a mean derivative equal to zero and low sample variance implied a high degree of connectivity. All calculations and basic statistics were performed using algorithms developed in MATLAB (MATLAB 6.0 Professional Version, MathWorks, Natick, MA).

Kinematics analysis of strain fields

Continuum kinematics analysis was used to determine whether local Z-disk strain fields were representative of strain fields across the entire fiber diameter. Homogeneous deformations (elongation, shortening, linear shear, and rotation) were applied to a subset of the two-dimensional confocal fiber images (n = 4 for +/+ and *des* −/−) to simulate passive loading computationally. The resulting images of the computationally strained fiber were subtracted from the corresponding actual images of the experimentally strained fiber, and difference images (i.e., error images) were systematically characterized. Successful predictions of fiber deformation consequently allowed quantification of fiber shear and fiber volume change. Details of

these calculations, which have been previously applied to analyze deformations in cardiac muscle (Mazhari and McCulloch, 2000; Mazhari et al., 1998), are provided in Appendices A and B.

Statistics

Linear and quadratic regressions and analyses of variance (ANOVA) were calculated using Statview 5.0 (Abacus, Berkeley, CA). Values are given in the text as mean ± SE.

RESULTS

Z-band-costamere interactions with increasing strain

For wild-type fibers, α-actinin staining resulted in the expected striation pattern, and cytoskeletal continuity across the fiber diameter (as seen by the ability to track individual Z-bands across the fiber diameter; Fig. 1). Though desmin-null fibers displayed α-actinin periodicity longitudinally, cytoskeletal continuity in the radial direction was not readily apparent, resulting in a disjointed fiber appearance (Fig. 2). For both wild-type and desmin-null fibers, talin labeling was periodic and localized to the cell membrane (Figs. 1 and 2). At increasing strains, in both genotypes, talin intensity profile peaks colocalized with α-actinin, with an additional talin peak maintaining its position halfway between consecutive Z-disks. Regression analysis confirmed that talin periodicity was one-half of the α-actinin periodicity (WT: $y = 0.51 \times -0.01, r^2 = 1.00$; KO: $y = 0.51 \times -0.01, r^2 = 0.99$; Fig. 3 *A*). At all strains and even at stresses exceeding 250 kPa (see below), there was a negligible phase shift between the talin and α-actinin peaks (Fig. 3 *B*) suggesting a rigid mechanical connection between the two structures.

Nuclear positioning and deformation with increasing strain

Individual nuclei, tracked at increasing fiber strains in both wild-type (Fig. 4) and knockout (Fig. 5) fibers, displayed the expected elliptical shape. In wild-type fibers, the nuclear aspect ratio (length/width) increased with strain, suggesting a coupling of nuclei and cytoskeletal structures (Figs. 4, *B–G*, and 6). In contrast, in desmin-null fibers, the coupling of nuclear aspect ratio to strain was markedly reduced, with aspect ratio increasing little, if at all, with sarcomere length (Figs. 5, *B–G*, and 6). The linear regression slope of nonnormalized aspect ratio versus SL curves for desmin-null nuclei was significantly lower ($p < 0.005$) compared to that of the wild-type nuclei (WT: 2.71 ± 0.34; KO: 1.16 ± 0.30). However, wild-type nuclei were significantly longer at resting sarcomere lengths and had a higher initial aspect ratio (length (μm), WT: 20.43 ± 0.82; KO: 14.65 ± 0.71; aspect ratio, WT: 3.84 ± 0.42; KO: 2.64 ± 0.15; $p < 0.05$). To ensure that differences in slope did not simply result from differences in initial aspect ratio, aspect ratios were normalized to initial aspect ratio, and still, significant differences ($p < 0.05$) were found between the regression slopes of the normalized aspect ratio versus SL relationship in desmin-null compared to wild-type nuclei (WT: 0.78 ± 0.09; KO: 0.42 ± 0.14; Fig. 6).

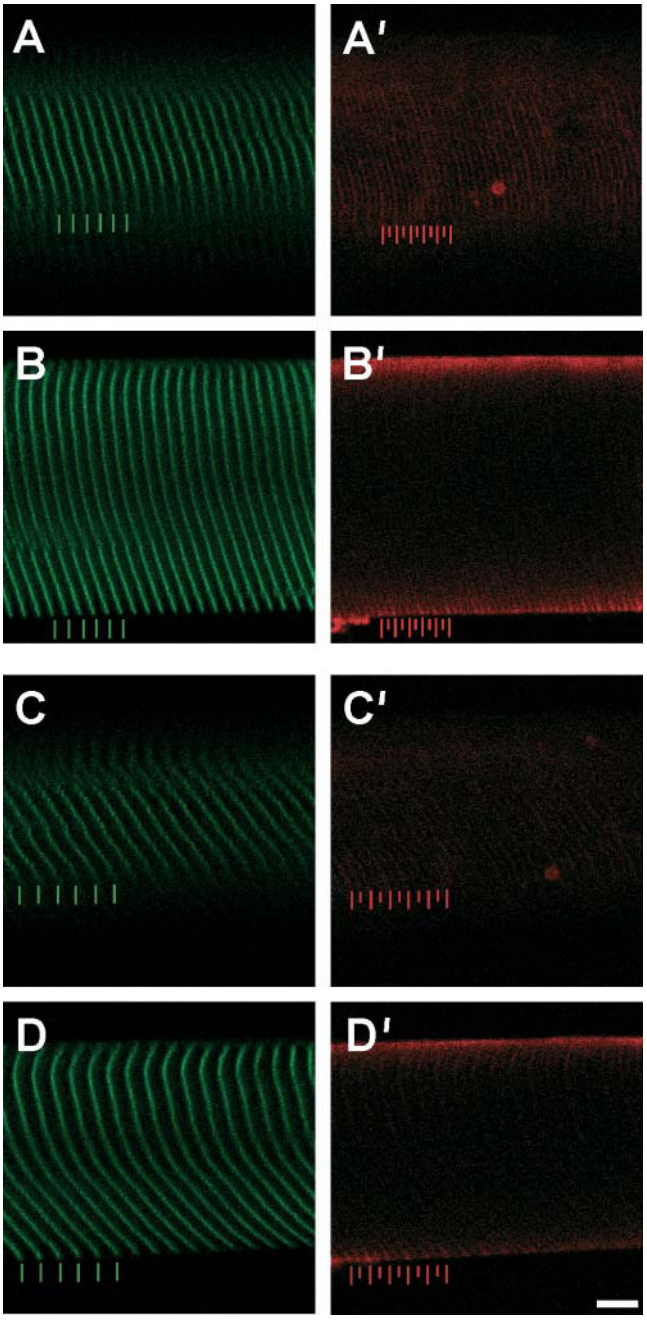

FIGURE 1 Sample wild-type fibers double labeled for α-actinin and talin are displayed at two different strains. (*A* and *B*) Sarcomere length ~2.80 μm. (*C* and *D*) Sarcomere length ~3.60 μm. Left frames (*A–D*) show α-actinin labeling (*green*) and right frames (*A′–D′*) show talin labeling (*red*). Upper frames (*A* and *C*) show superficial optical sections and lower panels (*B* and *D*) show deep optical sections. Periodicity and relative displacement of intensity peaks (i.e., localization) were determined by FFT and AC functions. Colored bars represent positions of peak intensity. Scale bar, 10 μm.

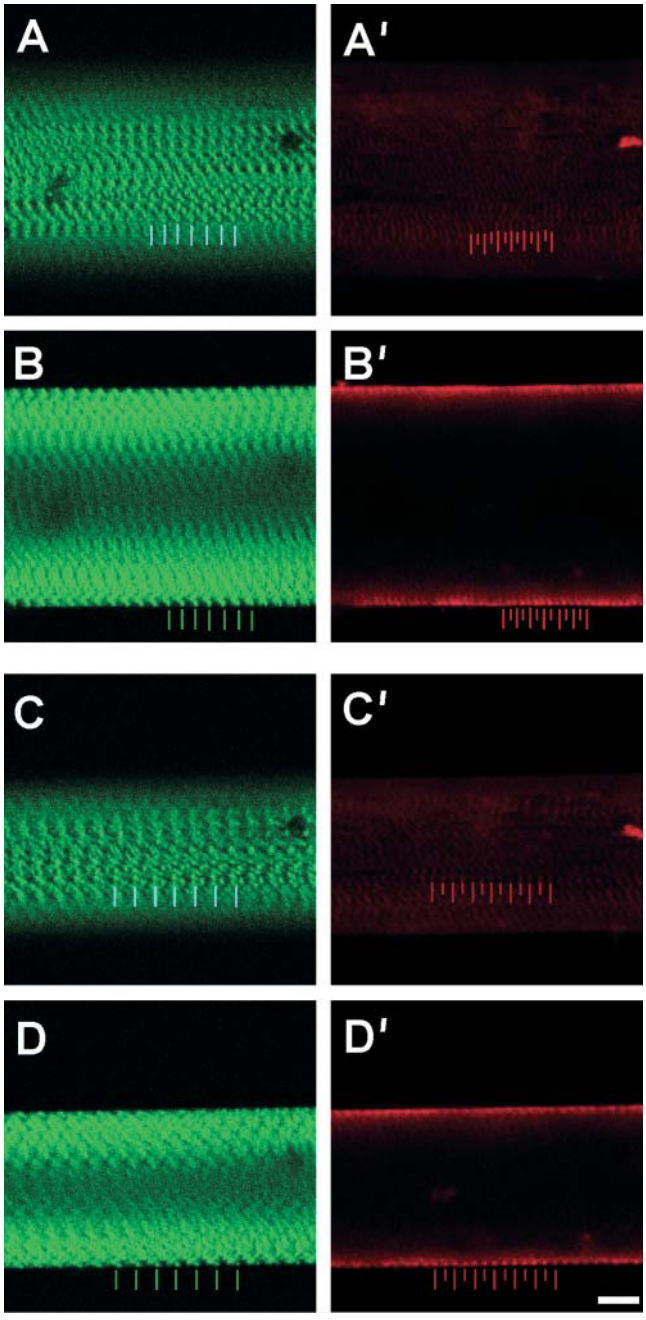

FIGURE 2 Sample desmin-null fibers double labeled for α-actinin and talin are displayed at two different strains. (*A* and *B*) Sarcomere length ~3.22 μm. (*C* and *D*) Sarcomere length ~4.09 μm. Left frames (*A–D*) show α-actinin labeling (*green*) and right frames (*A′–D′*) show talin labeling (*red*). Upper frames (*A* and *C*) show superficial optical sections and lower panels (*B* and *D*) show deep optical sections. Periodicity and relative displacement of intensity peaks (i.e., localization) were determined by FFT and AC functions. Colored bars represent positions of peak intensity. Scale bar, 10 μm.

The apparent uncoupling of individual nuclei from the cytoskeleton in the desmin-null fibers may reflect a large-scale change in nuclear positioning. To verify this, whole fibers were examined after fluorescent labeling of the nuclei with the dye Hoechst 33342. Perturbations in nuclear positioning were indeed observed in muscles with both fast and slow fiber types. The degree of perturbation was muscle dependent. In the soleus, segments with accumulations of nuclei as illustrated in Fig. 7 (SOL −/−) were observed in each of 20 fibers. They were interspersed with fiber segments of reduced nuclear density and with occasional normal-looking segments. This phenotype was already fully developed at 5 weeks. In the plantaris, segments of fibers with nuclear aggregates (Fig. 7, PL −/−) were present only in a subset of fibers at 5 weeks. These results directly show the importance of desmin for nuclear positioning in muscle fibers.

Myofibrillar connectivity with increasing strain

Mean phase shift variance across the fiber diameter was significantly higher for desmin-null fibers compared to wild-type fibers (WT: 0.023 ± 0.005; KO: 0.052 ± 0.006, $p < 0.005$), particularly at high sarcomere lengths (Fig. 8 *A*). Wild-type fibers displayed a phase shift difference variance close to zero at all strains, in sharp contrast to knockout fibers that demonstrated a relatively high phase shift variance across a range of strains (WT: 0.015 ± 0.006; KO: 0.078 ± 0.012; Fig. 8 *B*, $p < 0.001$).

Mechanical measurements

Cauchy stress was plotted against sarcomere length for each experiment, and fit using quadratic regression (r^2 for each individual curve >0.95; Fig. 9 *A*). All wild-type fibers (11 fibers) displayed a strong quadratic relationship between stress and sarcomere length, with the coefficient of the quadratic term of the regression line always having a value >15 (42.5 ± 2.5). Knockout fibers, on the other hand, were readily categorized into two distinct subgroups. Fibers from one subgroup (nine fibers) were significantly more compliant ($p < 0.05$) compared to wild-type fibers, though each had a quadratic regression coefficient value >15 (32.8 ± 4.37). Desmin-null fibers from the other subgroup (eight fibers) were significantly more compliant (4.15 ± 1.39) compared to both wild-type ($p < 0.0001$) and stiff knockout ($p < 0.0001$) fibers, with each coefficient of the regression quadratic term <10.

To determine whether differences in fiber populations were a result of changes in fiber geometry or overall load-bearing ability, LaGrangian stress was also plotted against sarcomere length for each fiber, and fit using quadratic regression (r^2 for each individual curve >0.98) and linear regression (r^2 for each individual curve >0.93; Fig. 9 *A*, *inset*). Use of the undeformed area to calculate stress had the effect of flattening the curves, so linear regression coefficients were compared. Slopes for wild-type fibers (32.08 ± 1.59) were again significantly different from stiff knockout fibers (25.62 ± 1.98; $p < 0.02$) as well as compliant knockout fibers (11.41 ± 1.10; $p < 0.0001$). Though the use of LaGrangian stress, by

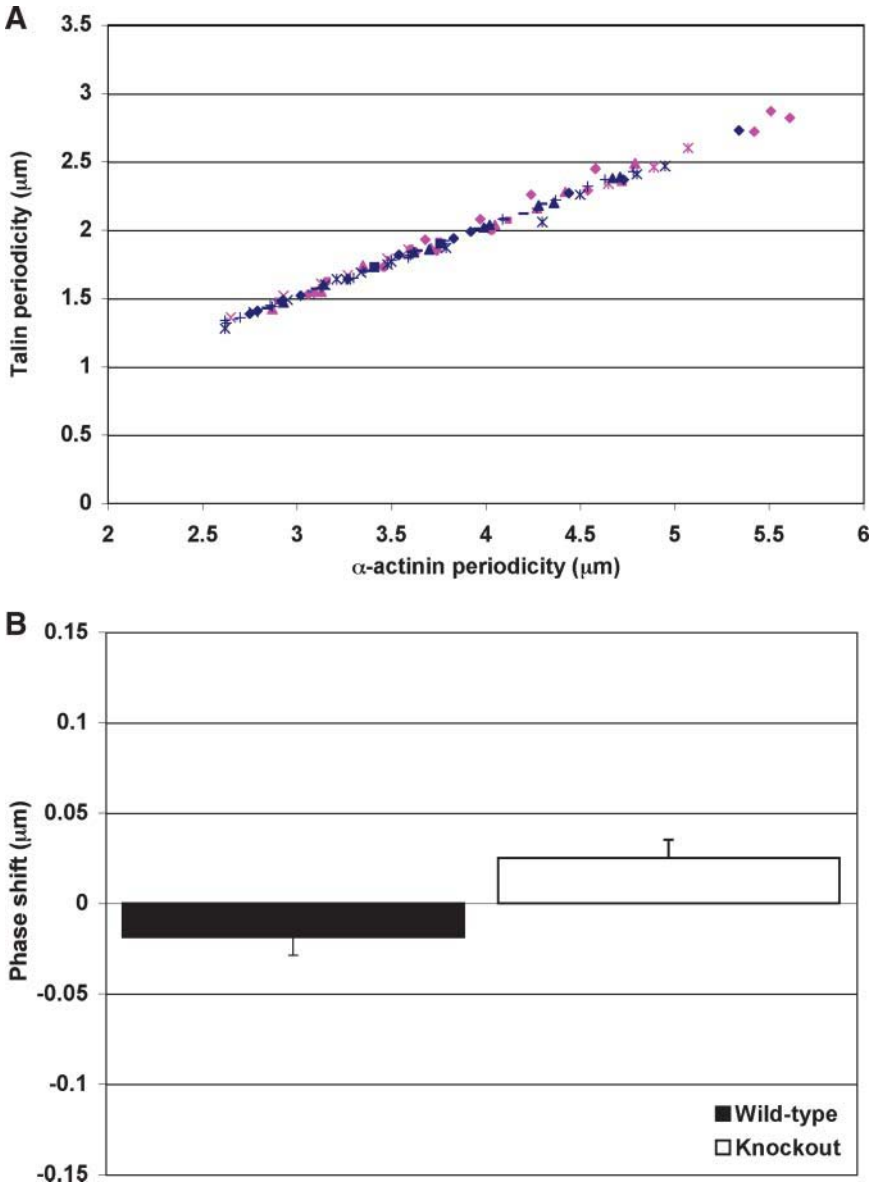

FIGURE 3 Talin colocalizes with α-actinin in wild-type and knockout fibers, suggesting that desmin is not essential for connecting costameres to the sarcomere lattice. (*A*) Periodicity of talin fluorescent intensity plotted versus α-actinin fluorescent intensity for wild-type (*pink*) and desmin-null (*blue*) fibers. α-Actinin periodicity is used to indicate sarcomere length. Different symbols of the same color represent different experiments. (*B*) Average phase shift between talin intensity profile and α-actinin intensity profile of data pooled from all sarcomere lengths for wild-type (*pink*) and desmin-null (*blue*) fibers. Note that these shifts are negligible compared to the pixel spacing, which is 0.14 μm.

definition, led to a decrease in the relative differences between mean linear and quadratic coefficients for the two groups of knockout fibers (data not shown), the fibers remained in two distinct groups ($p < 0.001$). Finally, to test whether the difference between groups was due to different amounts of residual extracellular matrix (ECM) adhering to the fibers, fibers from wild-type and knockout mice were treated with collagenase. Linear regression slopes of the LaGrangian stress-sarcomere length plots were compared, yielding the same effect of collagenase on both wild-type and knockout fibers, namely a significant decrease of 30% for each genotype ($p < 0.05$, $n = 8$ for each experimental group). This result is consistent with the fact that no desmin-null fibers with mechanical properties intermediate between the stiff and compliant groups were observed, as would be expected for varying amounts of ECM deposition on different fibers.

Analysis of radial strain as a function of sarcomere length provided further insight into the differences in load bearing between the subgroups of desmin-null fibers. Wild-type fibers and stiff knockout fibers demonstrated a similar inverse relationship between radial strain and sarcomere length whereas compliant knockout fibers exhibited a significantly weaker correlation ($p < 0.001$) between radial strain and sarcomere length (Fig. 9 *B*) compared to both wild-type and stiff knockout fibers.

In light of the altered radial response of a significant subset of desmin-null fibers to longitudinal loading, we attempted to determine the role desmin plays in response to osmotic compression. Compression of wild-type and knockout fibers with 8% dextran reversed any swelling occurring during the skinning effected by storage in glycerol and reflected compressive mechanical properties of the sarcomere lattice.

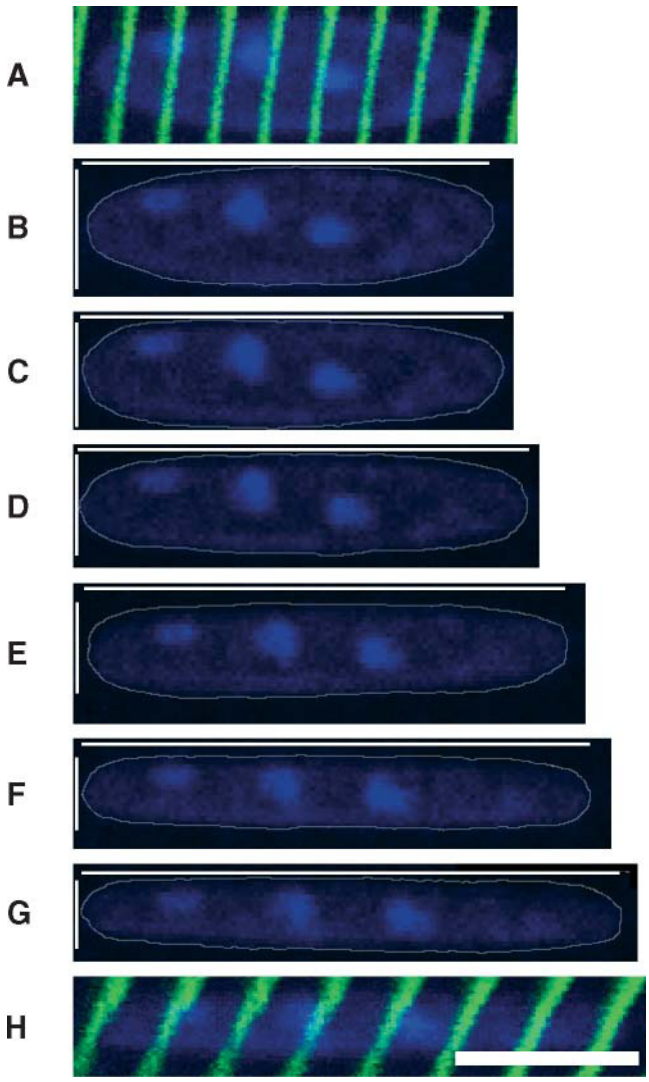

FIGURE 4 Sample wild-type nuclear labeling displayed at increasing fiber strain. Top frame (*A*) shows an overlay of α-actinin label on an unstretched nucleus whereas bottom frame (*H*) shows an overlay of α-actinin label on a maximally stretched nucleus. Sarcomere lengths in the region of the nucleus, measured using AC/FFT, were (*B*) 2.70 μm, (*C*) 2.98 μm, (*D*) 3.26 μm, (*E*) 3.43 μm, (*F*) 3.72 μm, and (*G*) 3.99 μm. Thin white lines indicate nuclear length and width. Nuclei (*blue*) are outlined using thin gray lines. Note the constant relative position of individual Z-disks (*green*) with respect to the nucleus. Scale bar, 10 μm.

Resting sarcomere lengths, which were consistent with previous resting lengths for the EDL (Burkholder et al., 1994; Burkholder and Lieber, 2001; James et al., 1995), were identical for wild-type and knockout fibers (KO: 2.89 $\pm$ 0.06, $n = 6$; WT: 2.93 $\pm$ 0.04, $n = 8$; $p > 0.6$). Diameters of uncompressed fibers were not significantly different (KO: 53.72 $\pm$ 3.88, $n = 6$; WT: 52.71 $\pm$ 1.69, $n = 8$; $p = 0.8$). However, knockout fibers experienced a significantly greater reduction in diameter (initial diameter/compressed diameter) when subject to a dextran-induced osmotic pressure (KO: 1.57 $\pm$ 0.03; WT: 1.39 $\pm$ 0.03; $p = 0.001$).

Mathematical modeling of fiber response to passive loading

Though the forces measured during mechanical loading of fiber segments were in the longitudinal direction, the nature of attachment of the fiber to the titanium wire prevented perfectly longitudinal application of force to individual myofibrils resulting in shear forces being applied to the fiber. To quantify these shear forces and to characterize the role of desmin in transmitting shear throughout the fiber, deformation gradient tensors (**F**) were predicted to simulate homogeneous deformation in two-dimensional longitudinal sections of the fiber for each stretch as described in Appendices A and B. Homogeneous deformations predicted fiber response to experimental passive loading accurately for both wild-type and knockout fibers (Fig. 10; Table 2). In fact, the magnitude of error in each case was less than the systematic error predicted by application of deformation to schematic muscle fibers (Appendix B, Table A1). Furthermore, there was a slight trend toward less error for desmin-null fibers compared to wild-type fibers, suggesting that the desmin-null sarcomere lattice actually deformed more homogeneously during stretch compared to the wild-type lattice. The successful prediction of fiber response to stretch by use of a homogeneous deformation permitted calculation of shear and fiber volume (longitudinal section area in two dimensions) by mathematical manipulation of the deformation gradient tensor (Table 2). Shear in knockout fibers was significantly reduced compared to wild-type fibers ($p < 0.005$). Area change was not significantly different in either group ($p > 0.25$), though there was a slight average increase in area in desmin-null fibers.

DISCUSSION

We utilized a novel experimental system that allowed simultaneous confocal imaging of fiber structure and measurement of passive mechanical properties to assess structural and functional roles of the intermediate filament desmin. We examined the interactions of three structures believed to be linked by the intermediate filament system: Z-disks, nuclei, and costamere protein complexes. In addition, we applied signal and image processing techniques to quantify structural connectivity and utilized a continuum kinematics model to simulate and predict fiber response to passive loading.

Desmin's role in connecting costameres to the sarcomere lattice

There is considerable debate regarding the identity and localization of costameric proteins within the sarcolemma, issues necessary to understand the coupling of the contractile apparatus to the sarcolemma and the extracellular matrix during repeated cycles of elongation and contraction (Pardo

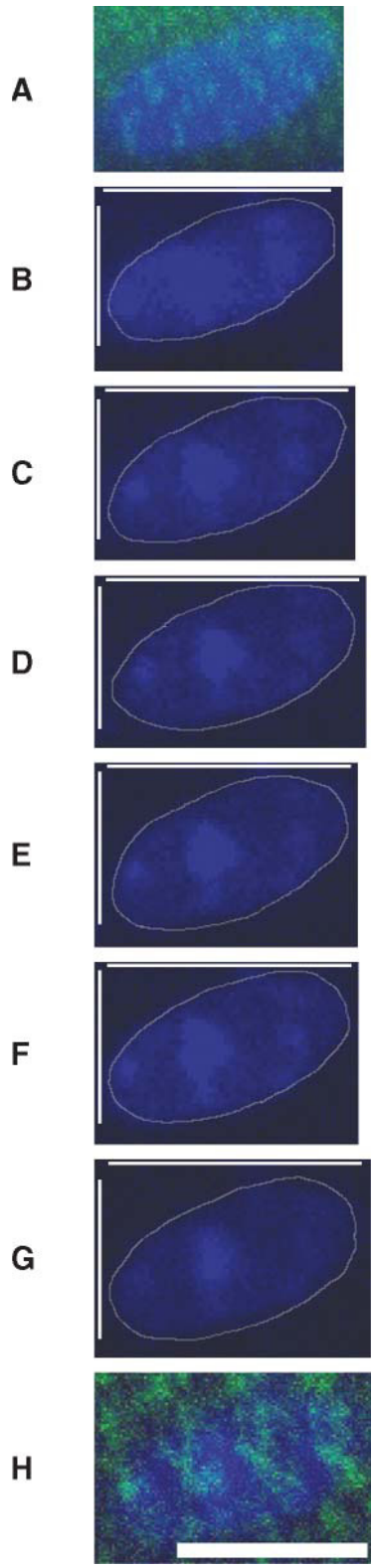

FIGURE 5 Sample desmin-null nuclear labeling displayed at increasing fiber strain. Top frame (*A*) shows an overlay of α-actinin label on an unstretched nucleus whereas bottom frame (*H*) shows an overlay of α-actinin label on a maximally stretched nucleus. Sarcomere lengths in the region of the nucleus, measured using AC/FFT, were (*B*) 2.55 μm, (*C*) 2.77 μm, (*D*) 3.04 μm, (*E*) 3.30 μm, (*F*) 3.52 μm, and (μ) 3.87 μm. Note the lack of an increase in aspect ratio (in contrast to Fig. 4). Thin white lines indicate nuclear length and width. Nuclei are outlined using thin gray lines. Scale bar, 10 μm.

et al., 1983a,b; Tidball et al., 1986). Pardo and colleagues demonstrated that, in chicken skeletal muscle, immunostaining for vinculin, believed to be a binding partner to talin within costamere complexes, localizes over the I-bands, with a transverse discontinuity at the Z-line and an absence staining at the M-line (Pardo et al., 1983b). On the other hand, Mondello et al. (1996) suggest that in human muscle, vinculin spans the entire Z-band/I-band region, whereas talin is observed at the Z-line and the M-line. Unfortunately, the latter study was performed with unspecified microscope objective properties in fibers fixed and frozen at sarcomere lengths of 2.5–2.7 μm, so the ability to accurately detect discontinuities between thick clusters of fluorescence is in question. Our analysis of talin localization in unfixed wild-type fibers revealed that talin colocalized with the Z-disk protein α-actinin, even at very high strains (Figs. 1 and 3 *B*). In addition, a second talin striation was observed between the Z-band talin striations. We believe that this striation is centered at the M-line, because the periodicity of talin is exactly half of that of α-actinin (Fig. 3 *A*; Table 1). Surprisingly, similar localization and periodicity of talin were observed in desmin-null fibers (Figs. 2 and 3; Table 1), even in the presence of considerable shear (Table 2). The possibility exists that the colocalization observed between talin and α-actinin is a result of a nonsarcomeric (costameric) α-actinin translating with each costamere during stretch. However, because the fluorescent focal planes, within which fibers exhibit significant curvature, are $\sim$ 2–3-μm thick, it is likely that a significant portion of the α-actinin label intensity profile originated in the myofibrils rather than the costameres.

Our data are consistent with a recent study reported by Bloch and colleagues (O'Neill et al., 2002), where costameres in desmin-null gastrocnemius and quadriceps muscles appeared to be stable. In addition, the half-sarcomere periodicity of talin is consistent with their observations of M-line costameres. Our study also resolves any questions raised due to potential imaging artifacts in localization analysis of fixed whole muscle sections. Our single-fiber system allows for alignment of each fiber in three dimensions, thereby preventing artifacts due to fiber obliqueness (e.g., systematic shifts in single label periodicity as well as relative displacements of multiple labels). Also, in light of unique protein localization patterns in deep and superficial sections of a muscle fiber (e.g., Figs. 1 and 2), our ability to determine the precise depth of the focal plane with respect to fiber diameter precludes potential bias due to variation in section depth across different samples. Finally, the utilization of signal processing functions to determine peak periodicity and peak phase shifts of intensity profiles prevents the possible misrepresentation of colocalization resulting from a qualita-

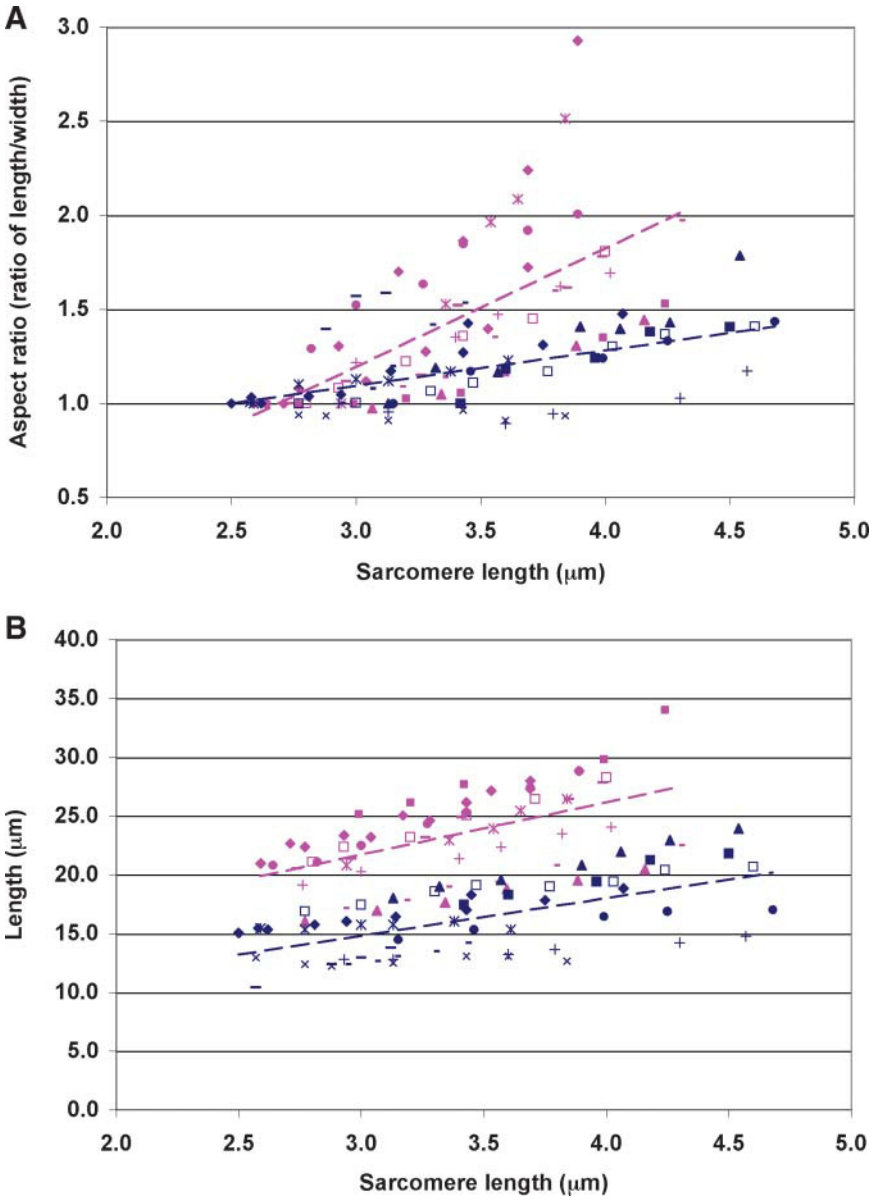

FIGURE 6 Desmin plays a role in regulating nuclear shape. (*A*) Plot of wild-type (*pink*) and desmin-null (*blue*) nuclear aspect ratio versus sarcomere length. Aspect ratios are normalized to the aspect ratio at resting sarcomere length. (*B*) Plot of wild-type (*pink*) and desmin-null (*blue*) nuclear length versus sarcomere length. Mean regression slopes are 4.45 for wild-type data and 3.19 for desmin-null data. Differences in nuclear geometry are evident at resting sarcomere length. Different symbols within a color group represent different experiments. Details on statistical differences between groups in this and subsequent figures are provided in text.

tive analysis of confocal images (e.g., a periodic ''green'' profile overlaid on a nonspecific ''red'' profile of constant intensity would appear visually to colocalize, but would not appear so quantitatively).

These data indicate that desmin is not essential for mechanical coupling of costamere complexes to the sarcomere lattice. Alternately, even in the absence of desmin-mediated connections, one of the host of other proteins and protein complexes in the membrane, including integrins, dystroglycan complexes, and other intermediate filaments, may help stabilize the interaction between the cell membrane and the cell cytoskeleton. In light of the variable localization of desmin, talin, vinculin (Pardo et al., 1983), and cytokeratins (O'Neill et al., 2002), it also seems increasingly likely that costamere complexes come in different varieties. It is plausible that, depending on the functional requirements of a given connection, the cast of proteins forming a costamere complex may be altered.

Desmin's role in myofibrillar connectivity and fiber geometry

Within the sarcomere lattice, significant differences in connectivity were revealed qualitatively and quantitatively between passively strained wild-type and desmin-null fibers (Figs. 1, 2, and 8). These findings confirmed hypothesized roles for desmin based on localization studies (Granger and Lazarides, 1979; Richardson et al., 1981; Tokuyasu et al., 1983; Wang and Ramirez-Mitchell, 1983). In addition, our results extended stereological findings at the ultrastructural

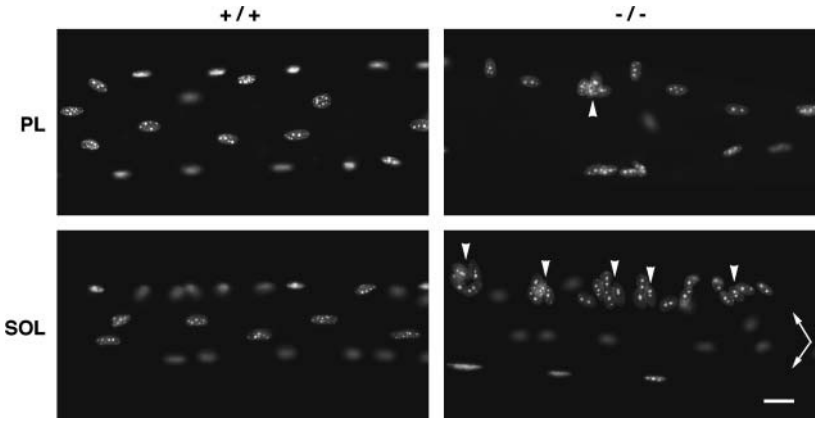

FIGURE 7 Desmin plays a role in nuclear localization in varying fiber types. Single fibers were prepared from the plantaris (PL) and soleus (SOL) muscles of 5-week-old control (+/+) and desmin-null (−/−) mice. They were stained with Hoechst 33342 to label the nuclei and observed under ultraviolet fluorescence. In +/+ fibers, nuclei are regularly distributed and often oriented longitudinally. In −/− fibers, their distribution is less regular and transverse orientation is frequent. Clusters of nuclei (*arrowheads*) are occasional in the plantaris but frequent in the soleus. The soleus −/− panel shows two fibers (*arrows*), one of which presents a normal-looking segment in this field. Bar, 20 μm.

level (Shah et al., 2002), providing objective measures of both local and fiber-wide myofibrillar connectivity at different sarcomere strains within the same specimen. In addition, we directly correlated myofibrillar connectivity with fiber geometry and mechanical function during passive loading.

Because fiber segments were lightly skinned during storage, the osmotic barrier thought to be responsible for regulating fiber volume was lost (Godt and Maughan, 1977). Even in the absence of this barrier, though, presumably due to extramyofibrillar connections, wild-type fibers still displayed a strong relationship between longitudinal and radial geometry (Fig. 9 *B*). Despite the plethora of connections governed by desmin within the sarcomere lattice (Fig. 8), a population of stiff desmin-null fibers, with radial strain-sarcomere length relationships similar to those of wild-type fibers, revealed that desmin was not entirely responsible for the maintenance of fiber volume and efficient transmission of passive strain (Fig. 9 *B*). In addition, a desmin-null cytoskeleton was still able to respond predictably to homogeneous deformations (Fig. 10 *B*; errors in Table 2).

On the other hand, a significant population of fibers (eight out of 17 fibers, 12 out of 25 experiments) displayed a weak relationship between radial and longitudinal geometry, suggesting that desmin is at least partially responsible for regulating fiber volume and mechanical properties (compliant knockout fibers, Fig. 9, *A* and *B*). A potential explanation for the observed reduction in diameter change with longitudinal stretch is the presence of shear strain, manifest in an imaging field of fixed dimensions by reorientation of the principal axes of the fiber rather than dimensional changes along the original axes. However, kinematic analysis of α-actinin strain fields revealed that knockout fibers transmitted significantly less shear strain than wild-type fibers, and did, in fact, experience a slight increase in fiber volume (Table 2). Furthermore, desmin-null fibers skinned by storage in a glycerol-based solution experienced significantly more osmotic compression. These results support the premise that desmin is necessary to optimally regulate cell volume upon loss of the cell osmotic barrier, a conceivable event not only during chemical membrane skinning, but physiologically after degeneration of skeletal muscle fibers (e.g., Fridén and Lieber, 1998; Hall-Craggs, 1974). In addition, these results provide a subcellular basis for the decoupling of longitudinal and radial properties reported in whole desmin-null diaphragm muscles (Boriek et al., 2001).

Desmin's role in muscle passive mechanical properties

Measured differences in mechanical properties between desmin-null and wild-type fibers are in sharp contrast to differences previously reported for desmin-null muscles. Although Anderson et al. (2001) reported increased passive stiffness in desmin-null soleus muscles, in our hands single desmin-null fibers in both compliant and stiff populations displayed increased passive compliance compared to wild-type fibers. As observed via the calculation of LaGrangian stress, these differences were not exclusively a result of differential responses of fiber cross-sectional area to longitudinal stretch, but rather, reflect inherent differences in force development by structural components within the muscle fiber. In addition, previous studies thus far have not indicated any upregulation of known intermediate filaments, including nestin and vimentin, the intermediate filaments closest in function to desmin (Li et al., 1997; Milner et al., 1996). These results would seem to indicate that any observed increases in muscle stiffness in the absence of desmin are not direct results of the loss of desmin, but a secondary effect of extracellular changes in desmin-null mice that may occur during repeated degeneration and regeneration cycles (e.g., Itagaki et al., 1995) or aging (c.f. Goldspink et al., 1994). Consequently, the current report offers a more accurate representation of muscle passive mechanical behavior, resulting exclusively from an absence of desmin.

It is unclear why desmin-null fibers separate into two mechanical populations. Fibers from both wild-type and desmin-null muscles were subject to identical conditions of

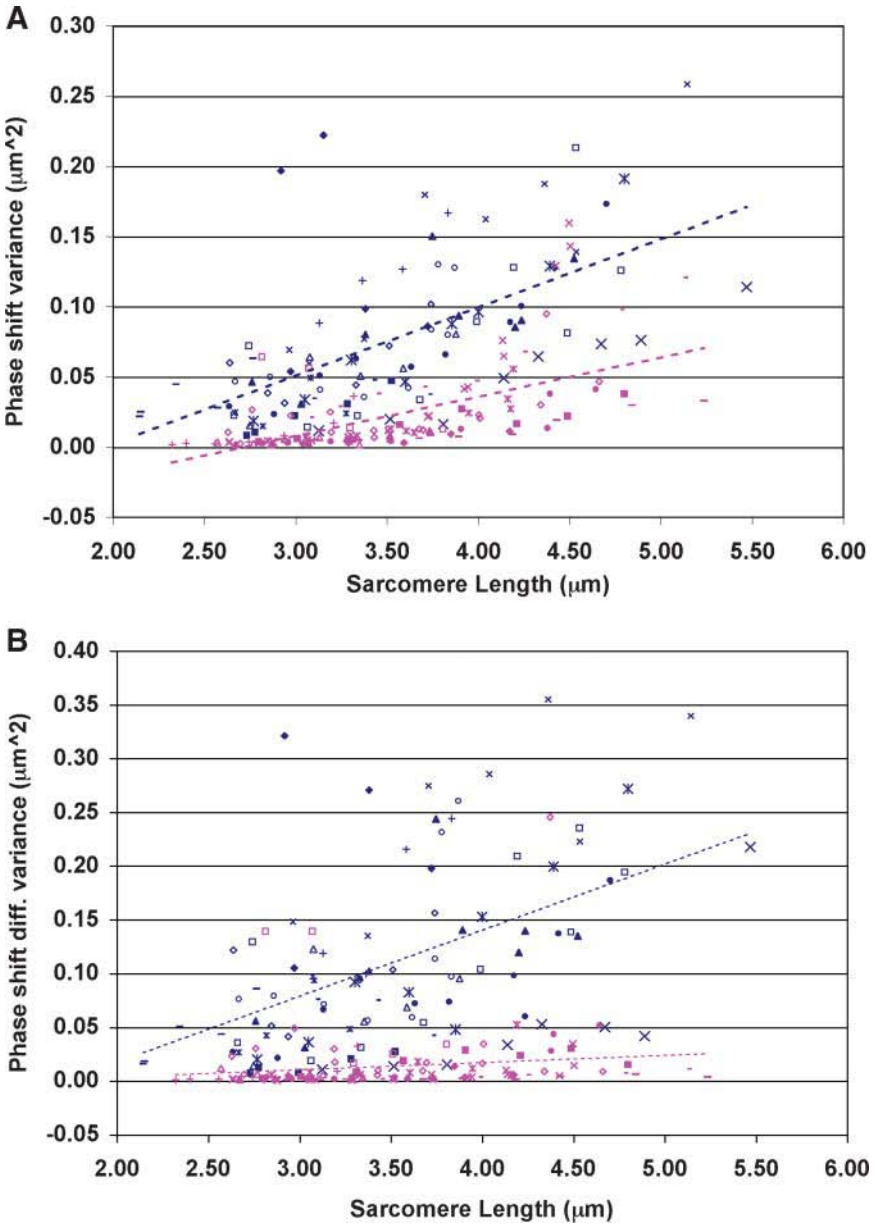

FIGURE 8 Desmin is required for myofibrillar connectivity. Connectivity plots of (*A*) phase shift variance and (*B*) phase shift difference variance versus sarcomere length for wild-type (*pink*) and desmin-null (*blue*) fibers. Panel *A* provides a measure of the homogeneity of connectivity across the fiber diameter, whereas *B* provides a measure of regional (myofibrillar) connectivity. Different symbols of the same color represent different experiments.

storage, dissection, and labeling. In addition, there was no observed correlation between the age or sex of the mice and the mechanical behavior of their fibers. Differences in relaxing solution pH or osmolarity are not likely to have affected the fiber mechanical properties, because groups of wild-type fibers were exposed to the same batch of solutions without any split in mechanical properties. Selective damage to desmin-null fibers during dissection or fiber mounting was also unlikely, as resting sarcomere lengths were not significantly different in any of the three groups of fibers, and inspection of the fluorescently labeled fibers before loading did not reveal any apparent abnormalities in α-actinin labeling along the fiber length. Treatment of fibers with collagenase excluded differences in the expression of type IV collagen, which is prevalent in the basement membrane that surrounds individual skeletal muscle cells (Hantai et al., 1983; Light and Champion, 1984). This result does not preclude the possible increase in other extracellular proteins, including the fibrillar collagens I and III. Studies are currently underway to parse out the contributions of specific extracellular proteins to passive tension, both in wild-type and desmin-null skeletal muscle.

Desmin's role in nuclear positioning and deformation

Whether intermediate filaments are physically integrated into the nuclear envelope in the different cell types studied and whether they form a continuous network with the nuclear matrix has been debated in the literature for quite some time

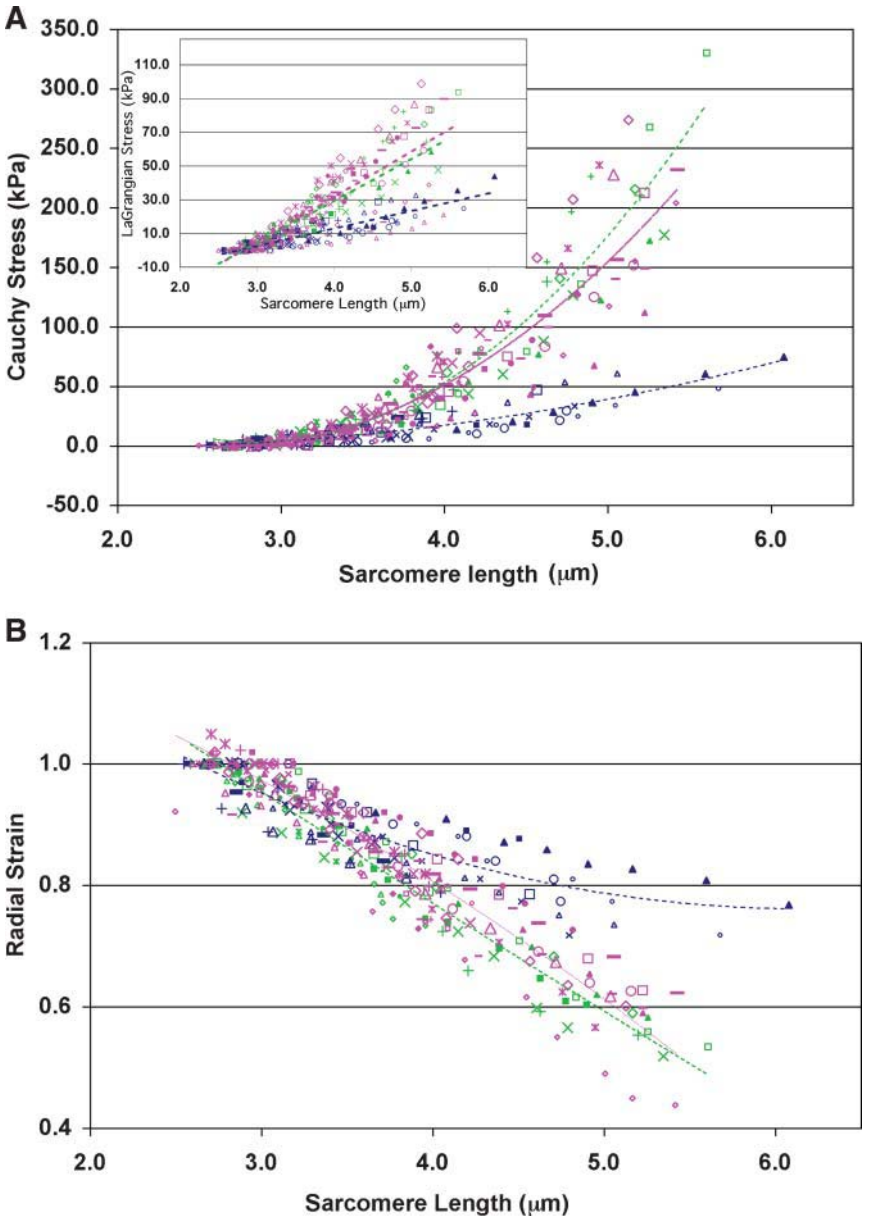

FIGURE 9 Desmin plays a role in passive stress bearing. Plots of (*A*) Cauchy stress (*inset*, LaGrangian stress) and (*B*) radial strain versus sarcomere length for wild-type fibers (*pink*, 25 experiments on 11 fibers), stiff desmin-null fibers (*green*, 13 experiments on nine fibers), and compliant desmin-null fibers (*blue*, 12 experiments on eight fibers). Divergence of stress-SL curves for wild-type or stiff knockout fibers and compliant knockout fibers occur at ~3.5–3.8 μm. Different symbols of the same color represent different experiments.

(for review see Georgatos and Maison, 1996; Capetanaki, 1997). Transmission electron microscopy has suggested that arrays of IFs could anchor ''end-on'' at the nuclear pores or they could make tangential contacts with the nuclear envelope (Franke, 1971; Harris and Brown, 1971; Lehto et al., 1978; Woodcock, 1980; Jones et al., 1982; Goldman et al., 1985). Furthermore, whole-mount EM on nuclear matrix preparations in different cell types has strongly suggested that indeed the cytoplasmic IFs form a continuous network with the nuclear lamina meshwork and that they could also connect to the nuclear pores via short, ~5-nm-thick fibers (Capco et al., 1982; Fey et al., 1984; Katsuma et al., 1987; Carmo-Fonseca et al., 1988, 1990; French et al., 1989; Fujitani et al., 1989; Wang et al., 1989). Biochemical studies have also shown that desmin, vimentin, and peripherin bind to lamin B of the karyoskeleton through their carboxy-termini (Georgatos and Blobel, 1987; Georgatos et al., 1987; Djabali et al., 1991; Papamarcaki et al., 1991). Finally, the existence of a transcellular desmin-lamin B filament network has also been reported for cardiac myocytes (Lockard and Bloom, 1993)). Based on the above and other data, it has been proposed that the IFs form part of a network that connects the extracellular and the nuclear matrix and thus could participate in mechanochemical signaling to the nucleus both from the outside of the cell as well as, in the case of muscle, from the contractile apparatus.

Additional support for transmembrane interactions between cytoplasmic IFs and intranuclear structures is provided by the widely observed modulation of nuclear architecture by IFs in different cell types. In cardiac and

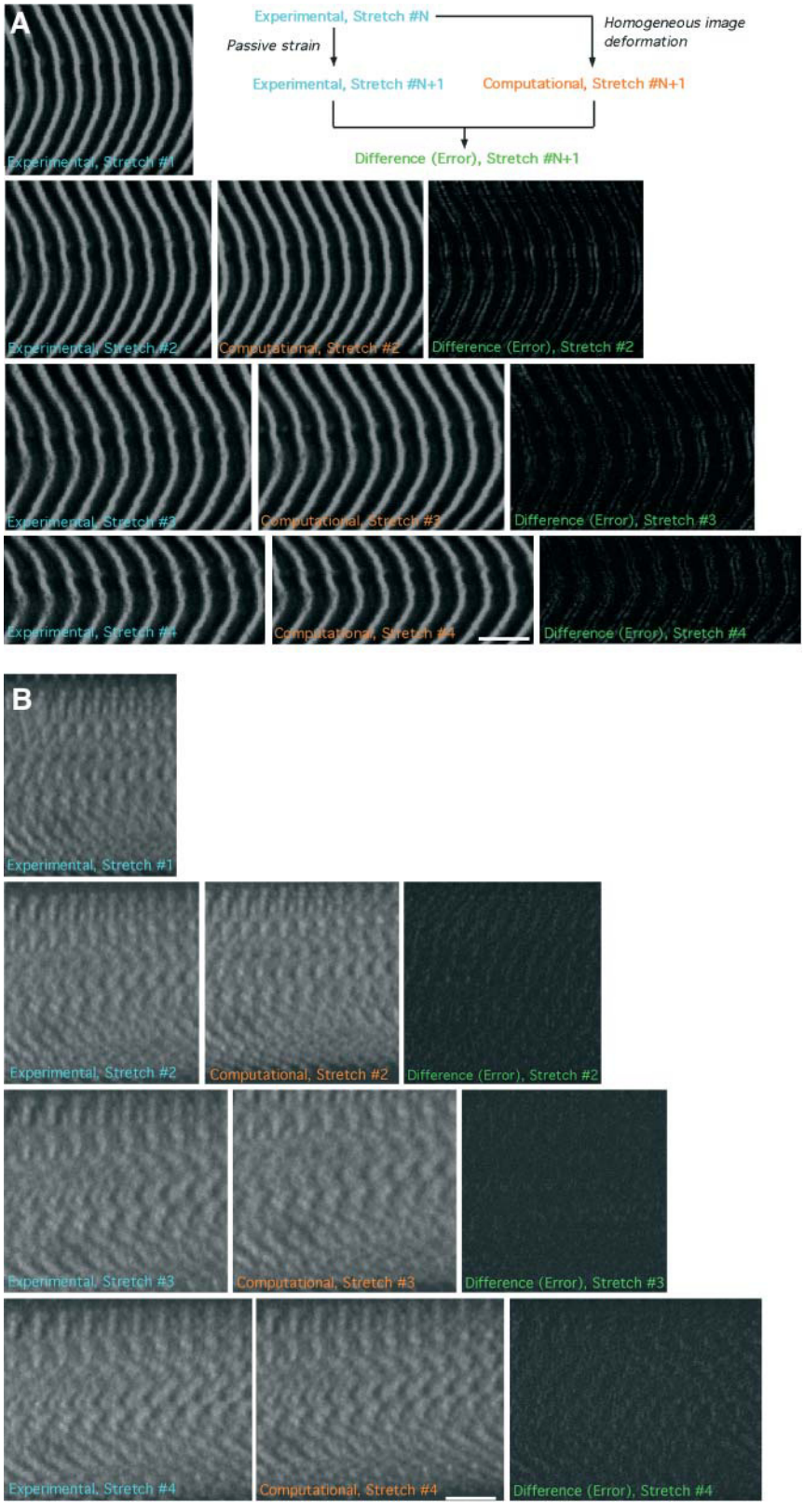

FIGURE 10 Sample images of a sequence of experimental and simulated passive stretches for (*A*) wild-type and (*B*) desmin-null fibers. Difference (error) images reveal that for both wild-type and desmin-null fibers, homogeneous deformations accurately predict fiber response. Scale bar, 10 μm.

TABLE 2 Error, shear, and area calculations (mean ± SE)

	Difference error (raw)	Maximum shear	Area change	Cumulative shear from five deformations	Cumulative shear from six deformations
WT	0.012 ± 0.002	0.083 ± 0.005	1.00 ± 0.01	0.394 ± 0.014	0.480 ± 0.026
KO	0.011 ± 0.001	0.065 ± 0.003*	1.02 ± 0.01	0.350 ± 0.013*	0.410 ± 0.020*

*Significant difference between wild-type and knockout.

skeletal muscle it is known that the nuclei of muscle fiber cells possess regularly spaced indentations that seem to be in register with the Z-lines of neighboring myofibrils and are presumably anchorage sites of the Z-disk-associated desmin filaments. It is also known that the shape and surface morphology of muscle nuclei change during muscle contraction and relaxation (Bloom and Cancillia, 1969). Thus, it may be speculated that desmin filaments anchoring to the nucleus could pull the nuclear envelope. The simplest interpretation of such data is that the cytoplasmic IFs actively stretch the nuclear envelope and/or the arrangement of the underlying heterochromatin. Such deformation has been correlated with intranuclear events such as gene expression and chromosomal arrangement (Chen et al., 1997; Croft et al., 1999; Lelievre and Bissell, 1998; review by Maxwell and Hendzel, 2001; Stein et al., 1999, 1998).

We tested the role of desmin in initiating such pathways via direct visualization of muscle nuclei before and during mechanical loading. Nuclear shape and nuclear response to deformation were both altered in the absence of desmin (Figs. 4–6). In addition, visualization of the nuclei in whole fibers from different muscles revealed a generalized perturbation in their position and orientation, stressing the necessity of desmin for the maintenance of nuclear positioning.

CONCLUSIONS

This study confirmed the relevance of cytoskeletal connectivity to skeletal muscle function, at a subcellular level. We demonstrated that desmin is important for the maintenance of nuclear positioning and transmission of mechanical loads through the cytoskeleton, though it is likely not essential for transmitting loads from the ECM/membrane to the sarcomere lattice periphery. Effective propagation of mechanical signals through the cell has significant implications for force transmission and the initiation of signal transduction cascades within the fiber and the nucleus.

APPENDIX A: KINEMATICS

Deformations in two dimensions may be represented by the matrix

$$x' = \mathbf{F}x, \tag{1}$$

where x' is a vector representing the coordinates of homogeneous deformed data points, x is a vector representing the material coordinates (undeformed data points), and $\mathbf{F}$ is the homogeneous deformation gradient tensor. To calculate the degree of shear and the area change of the two-dimensional imaged region, a series of tensor manipulations were performed (adapted from Spencer, 1980):

The Green deformation tensor $\mathbf{C}$ may be determined from $\mathbf{F}$ by

$$\mathbf{C} = \mathbf{F}^{\mathrm{T}}\mathbf{F} = \mathbf{S}\Lambda^2\mathbf{S}^{-1}, \tag{2}$$

where the eigenvalues of $\mathbf{C}$ (λ_1^2 and λ_2^2) are found in the diagonal matrix $\mathbf{L}$, and the eigenvectors (S_1 and S_2) are found as the columns in the orthogonal matrix $\mathbf{S}$. The stretch tensor $\mathbf{U}$ may be then calculated from the positive square root of $\mathbf{C}$:

$$\mathbf{U} = \mathbf{S}\Lambda\mathbf{S}^{\mathrm{T}} \tag{3}$$

Physically, the eigenvectors of $\mathbf{U}$ (and $\mathbf{C}$), $\mathbf{S}$, designate the principal strain axes relative to the material coordinates, and the eigenvalues of $\mathbf{U}$ (λ_1 and λ_2) designate the principal strains. From these eigenvalues, we may then calculate the change in area from the undeformed state to the deformed state as:

$$A = \lambda_1\lambda_2, \tag{4}$$

and the maximum shear $\gamma_{\max}$ for a given deformation as:

$$\gamma_{\max} = 0.5(\lambda_1 - \lambda_2). \tag{5}$$

These expressions may also be applied to calculate the cumulative change in area and shear for a number of consecutive deformations. For n deformations,

$$x' = \mathbf{F}_{\mathrm{n}}\mathbf{F}_{\mathrm{n-1}}\mathbf{F}_{\mathrm{n-2}}\ldots\mathbf{F}_1 x = \mathbf{F}_{\mathrm{c}}x, \tag{6}$$

where the cumulative deformation $\mathbf{F}_{\mathrm{c}}$ is the product of the individual deformations $\mathbf{F}_{\mathrm{i}}$. The remaining calculations then follow as described above.

APPENDIX B: DETERMINATION OF F AND ERROR ANALYSIS

An initial guess was made for $\mathbf{F}$ by manually selecting eight to 10 control points (points that were tracked from the confocal image of the undeformed fiber to that of the deformed fiber) and applying a Matlab function utilizing a least-square error algorithm in conjunction with the linear set of equations (see Eq. 1) to determine the four components of $\mathbf{F}$. To account for any error potentially resulting from manual selection of control points, the initial

TABLE A1 Table of difference errors for varying ratios of schematic Z-disks to inter-Z-disk widths (*R*), in the range of 10% longitudinal strain

Longitudinal strain	$R = 0.5$	$R = 0.75$	$R = 1.0$	$R = 1.25$	$R = 1.5$	$R = 2.0$
1.04	0.02	0.01	0.01	0.01	0.01	0.01
1.06	0.02	0.01	0.02	0.02	0.02	0.02
1.08	0.02	0.02	0.02	0.02	0.02	0.02
1.1	0.03	0.03	0.02	0.02	0.02	0.02
1.12	0.03	0.03	0.03	0.03	0.03	0.03
1.14	0.03	0.03	0.03	0.03	0.03	0.03
1.16	0.04	0.03	0.03	0.03	0.04	0.03

prediction was refined by systematically varying each of the components of **F** over a range of ±2% from the original value. Each of these deformations was applied to the image of the undeformed fiber, and the absolute value of the difference error (the mean pixel value of the difference image) between the computationally and experimentally generated stretch images was minimized to determine the optimal deformation gradient tensor.

Because a homogeneous deformation was applied to the entire fiber longitudinal section, the implicit assumption was made that the stiffness of the Z-band was identical to that of the region between Z-bands. Because in practice the Z-band is more likely to have a higher stiffness than the region between Z-bands, the difference image would consequently reveal a consistent increase in thickness of the Z-band in the image of computational stretch. To test this hypothesis, the difference error image was further characterized to determine whether the remaining error was systematic, as expected, or random. For each row of pixels across the fiber diameter, the ratio of error thickness (sum of error intensity) to computational Z-disk thickness (sum of Z-disk intensity) was determined per Z-disk (i.e., a measure of the percentage of the computationally stretched Z-disk thickness not explained by actual Z-band thickness). A systematic error would then be reflected by a constant ratio across the fiber diameter, whereas random error would be reflected by a ratio with a high variance across the fiber diameter.

To provide a reference point for the magnitude of errors generated by the homogeneous deformation of experimental images, the error characterization algorithm was first applied to schematic images of alternating white and black lines, representing Z-disks and the region between Z-disks, respectively. The ratio of the widths of these lines was varied to simulate fibers at a range of sarcomere lengths. Stretch was then applied either homogeneously, to simulate computational deformation, or only to the region between the Z-disks (thereby assuming Z-disks with infinite stiffness), to simulate experimental deformation, and the ratio of error thickness per Z-disk was calculated as described above. The range of simulation error values for sarcomere strains similar to those applied experimentally is presented in Table A1. It should be noted that in practice, due to limitations in axial confocal resolution, fluorescence from several layers of myofibrils is captured in a given confocal slice. Therefore, any misalignment or shearing of myofibrils in different planes may be manifest as an increase in Z-disk width. This artifact may be enhanced in the more mobile desmin-null myofibrils (Shah et al., 2002).

We thank Dr. Jan Fridén and Dr. Gordon Lutz for helpful discussions. We also thank Pat Reid and Dr. Jerry Vandeberg of the Veterans Affairs Healthcare Systems, San Diego, CA, core microscope facility. The generous support of National Institutes of Health (grants AR40050 and T32HL07089), the National Science Foundation, and Department of Veterans Affairs Rehabilitation Research and Development is greatly appreciated.

REFERENCES

Anderson, J., Z. Li, and F. Goubel. 2001. Passive stiffness is increased in soleus muscle of desmin knockout mouse. *Muscle Nerve*. 24:1090–1092.

Bloom, S., and P. A. Cancillia. 1969. Conformational changes in myocardial nuclei of rats. *Circ. Res.* 24:189–196.

Boriek, A. M., Y. Capetanaki, W. Hwang, T. Officer, M. Badshah, J. Rodarte, and J. G. Tidball. 2001. Desmin integrates the three-dimensional mechanical properties of muscles. *Am. J. Physiol. Cell Physiol.* 280:C46–C52.

Burkholder, T. J., B. Fingado, S. Baron, and R. L. Lieber. 1994. Relationship between muscle fiber types and sizes and muscle architectural properties in the mouse hindlimb. *J. Morphol.* 220:1–14.

Burkholder, T. J., and R. L. Lieber. 2001. Sarcomere length operating range of muscles during movement. *J. Exp. Biol.* 204:1529–1536.

Capco, D. G., K. M. Wan, and S. Penman. 1982. The nuclear matrix: three-dimensional architecture and protein composition. *Cell.* 29:847–858.

Capetanaki, Y., D. J. Milner, and G. Weitzer. 1997. Desmin in muscle formation an maintenance: knockouts and consequences. *Cell Struct. Funct.* 22:103–116.

Carmo-Fonseca, M, A. J. Cidadao, and J. F. David-Ferreira. 1988. Filamentous cross-bridges link intermediate filaments to the nuclear pore complexes. *Eur. J. Cell. Biol.* 45:282–290.

Carmo-Fonseca, M., and J. F. David-Ferreira. 1990. Interactions of intermediate filaments with cell structures. *Electron Microsc. Rev.* 3:115–141.

Chen, C. S., M. Mrksich, S. Huang, G. M. Whitesides, and D. E. Ingber. 1997. Geometric control of cell life and death. *Science.* 276:1425–1428.

Croft, J. A., J. M. Bridger, S. Boyle, P. Perry, P. Teague, and W. A. Bickmore. 1999. Differences in the localization and morphology of chromosomes in the human nucleus. *J. Cell Biol.* 145:1119–1131.

Danowski, B. A., K. Imanaka-Yoshida, J. M. Sanger, and J. W. Sanger. 1992. Costameres are sites of force transmission to the substratum in adult rat cardiomyocytes. *J. Cell Biol.* 118:1411–1420.

Djabali, K., M. M. Portier, F. Gros, G. Blobel, and S. D. Georgatos. 1991. Network antibodies identify nuclear lamin B as a physiological attachment site for peripherin intermediate filaments. *Cell.* 64:109–121.

Fey, E. G., K. M. Wan, and S. Penman. 1984. Epithelial cytoskeletal framework and nuclear matrix-intermediate filament scaffold: three-dimensional organization and protein composition. *J. Cell Biol.* 98:1973–1984.

Franke, W. W. 1971. Relationship of nuclear membranes with filaments and microtubules. *Protoplasma.* 73:263–292.

French, S. W., H. Kawahara, Y. Katsuma, M. Ohta, and S. H. Swierenga. 1989. Interaction of intermediate filaments with nuclear lamina and cell periphery. *Electron Microsc. Rev.* 2:17–51.

Fridén, J., and R. L. Lieber. 1998. Segmental muscle fiber lesions after repetitive eccentric contractions. *Cell Tissue Res.* 293:165–171.

Fujitani, Y., S. Higaki, H. Sawada, and K. Hirosawa. 1989. Quick-freeze, deep-etch visualization of the nuclear pore complex. *Electron Microsc. Rev.* 38:34–40.

Georgatos, S. D., and G. Blobel. 1987. Lamin B constitutes an intermediate filament attachment site at the nuclear envelope. *J. Cell Biol.* 2:117–125.

Georgatos, S. D., and C. Maison. 1996. Integration of intermediate filaments into cellular organelles. *Int. Rev. Cytol.* 164:91–138.

Georgatos, S. D., K. Weber, N. Geisler, and G. Blobel. 1987. Binding of two desmin derivatives to the plasma membrane and the nuclear envelope of avian erythrocytes: evidence for a conserved site-specificity in intermediate filament-membrane interactions. *Proc. Natl. Acad. Sci. USA.* 84:6780–6784.

Goldman, R., A. Goldman, K. Green, J. Jones, N. Lieska, and H. Y. Yang. 1985. Intermediate filaments: possible functions as cytoskeletal connecting links between the nucleus and the cell surface. *Ann. N. Y. Acad Sci.* 455:1–17.

Godt, R. E., and D. W. Maughan. 1977. Swelling of skinned muscle fibers of the frog. Experimental observations. *Biophys. J.* 19:103–116.

Goldspink, G., K. Fernandes, P. E. Williams, and D. J. Wells. 1994. Age-related changes in collagen gene expression in the muscles of mdx dystrophic and normal mice. *Neuromuscul. Disord.* 4:183–191.

Granger, B. L., and E. Lazarides. 1979. Desmin and vimentin coexist at the periphery of the myofibril Z disc. *Cell.* 18:1053–1063.

Granzier, H., and T. Irving. 1995. Passive tension in cardiac muscle: contribution of collagen, titin, microtubules, and intermediate filaments. *Biophys. J.* 68:1027–1044.

Harris, J. R., and J. N. Brown. 1971. Fractionation of the avian erythrocyte: an ultrastructural study. *J. Ultrastruct. Res.* 36:8–23.

Hall-Craggs, E. C. 1974. Rapid degeneration and regeneration of a whole skeletal muscle following treatment with bupivacaine (Marcain). *Exp. Neurol.* 43:349–358.

Hantai, D., J. Gautron, and J. Labat-Robert. 1983. Immunolocalization of fibronectin and other macromolecules of the intercellular matrix in the striated muscle fiber of the adult rat. *Coll. Relat. Res.* 3:381–391.

Itagaki, Y., K. Saida, and K. Iwamura. 1995. Regenerative capacity of mdx mouse muscles after repeated applications of myo-necrotic bupivacaine. *Acta Neuropathol.* 89:380–384.

James, R. S., J. D. Altringham, and D. F. Goldspink. 1995. The mechanical properties of fast and slow skeletal muscles of the mouse in relation to their locomotory function. *J. Exp. Biol.* 196:491–502.

Jones, J. C., A. E. Goldman, P. M. Steinert, S. Yuspa, and R. D. Goldman. 1982. Dynamic aspects of the supramolecular organization of intermediate filament networks in cultured epidermal cells. *Cell Motil.* 2:197–213.

Katsuma, Y., S. H. Swierenga, N. Marceau, and S. W. French. 1987. Connections of intermediate filaments with the nuclear lamina and the cell periphery. *Biol. Cell.* 59:193–203.

Lehto, V. P., I. Virtanen, and P. Kurki. 1978. Intermediate filaments anchor the nuclei in nuclear monolayers of cultured human fibroblasts. *Nature.* 272:175–177.

Lelievre, S. A., and M. J. Bissell. 1998. Communication between the cell membrane and the nucleus: role of protein compartmentalization. *J. Cell. Biochem. Suppl.* 31:250–263.

Li, Z., M. Mericskay, O. Agbulut, G. Butler-Browne, L. Carlsson, L. E. Thornell, C. Babinet, and D. Paulin. 1997. Desmin is essential for the tensile strength and integrity of myofibrils but not for myogenic commitment, differentiation, and fusion of skeletal muscle. *J. Cell Biol.* 139:129–144.

Lieber, R. L., Y. Yeh, and R. J. Baskin. 1984. Sarcomere length determination using laser diffraction. Effect of beam and fiber diameter. *Biophys. J.* 45:1007–1016.

Light, N., and A. E. Champion. 1984. Characterization of muscle epimysium, perimysium and endomysium collagens. *Biochem. J.* 219: 1017–1026.

Lockard, V. G., and S. Bloom. 1993. Trans-cellular desmin-lamin B intermediate filament network in cardiac myocytes. *J. Mol. Cell Cardiol.* 25:303–209.

Maniotis, A. J., C. S. Chen, and D. E. Ingber. 1997. Demonstration of mechanical connections between integrins, cytoskeletal filaments, and nucleoplasm that stabilize nuclear structure. *Proc. Natl. Acad. Sci. USA.* 94:849–854.

Maxwell, C. A., and M. J. Hendzel. 2001. The integration of tissue structure and nuclear function. *Biochem. Cell Biol.* 79:267–274.

Mazhari, R., and A. D. McCulloch. 2000. Integrative models for understanding the structural basis of regional mechanical dysfunction in ischemic myocardium. *Ann. Biomed. Eng.* 28:979–990.

Mazhari, R., J. H. Omens, L. K. Waldman, and A. D. McCulloch. 1998. Regional myocardial perfusion and mechanics: a model-based method of analysis. *Ann. Biomed. Eng.* 26:743–755.

Milner, D. J., M. Mavroidis, N. Weisleder, and Y. Capetanaki. 2000. Desmin cytoskeleton linked to muscle mitochondrial distribution and respiratory function. *J. Cell Biol.* 150:1283–1298.

Milner, D. J., G. Weitzer, D. Tran, A. Bradley, and Y. Capetanaki. 1996. Disruption of muscle architecture and myocardial degeneration in mice lacking desmin. *J. Cell Biol.* 134:1255–1270.

Mondello, M. R., P. Bramanti, G. Cutroneo, G. Santoro, D. Di Mauro, and G. Anastasi. 1996. Immunolocalization of the costameres in human skeletal muscle fibers: confocal scanning laser microscope investigations. *Anat. Rec.* 245:481–487.

O'Neill, A., M. W. Williams, W. G. Resneck, D. J. Milner, Y. Capetanaki, and R. J. Bloch. 2002. Sarcolemmal organization in skeletal muscle lacking desmin: evidence for cytokeratins associated with the membrane skeleton at costameres. *Mol. Biol. Cell.* 13:2347–2359.

Papamarcaki, T., P. D. Kouklis, T. E. Kreis, and S. D. Georgatos. 1991. The ''lamin B-fold''. Anti-idiotypic antibodies reveal a structural complementarity between nuclear lamin B and cytoplasmic intermediate filament epitopes. *J. Biol. Chem.* 266:21247–21251.

Pardo, J. V., J. D. Siliciano, and S. W. Craig. 1983a. Vinculin is a component of an extensive network of myofibril-sarcolemma attachment regions in cardiac muscle fibers. *J. Cell Biol.* 97:1081–1088.

Pardo, J. V., J. D. Siliciano, and S. W. Craig. 1983b. A vinculin-containing cortical lattice in skeletal muscle: transverse lattice elements (''costameres'') mark sites of attachment between myofibrils and sarcolemma. *Proc. Natl. Acad. Sci. USA.* 80:1008–1012.

Richardson, F. L., M. H. Stromer, T. W. Huiatt, and R. M. Robson. 1981. Immunoelectron and immunofluorescence localization of desmin in mature avian muscles. *Eur. J. Cell Biol.* 26:91–101.

Sam, M., S. Shah, J. Fridén, D. J. Milner, Y. Capetanaki, and R. L. Lieber. 2000. Desmin knockout muscles generate lower stress and are less vulnerable to injury compared to wildtype muscles. *Am. J. Physiol.* 279:C1116–C1122.

Shah, S., J. Fridén, F.-C. Su, D. J. Milner, Y. Capetanaki, and R. L. Lieber. 2002. Evidence for increased mobility of myofibrils in desmin null skeletal muscles. *J. Exp. Biol.* 205:321–325.

Shah, S., and R. L. Lieber. 2003. Real-time imaging and mechanical measurement of muscle cytoskeletal proteins. *J. Histochem. Cytochem.* 51:19–29.

Spencer, A. J. M. Continuum Mechanics, London, England. Longman Group Limited, 1980.

Stein, G. S., A. J. Van Wijnen, M. Montecino, J. L. Stein, and J. B. Lian. 1999. Nuclear structure/gene expression interrelationships. *J. Cell. Physiol.* 181:240–250.

Stein, G. S., A. J. van Wijnen, J. L. Stein, J. B. Lian, S. Pockwinse, and S. McNeil. 1998. Interrelationships of nuclear structure and transcriptional control: functional consequences of being in the right place at the right time. *J. Cell. Biochem.* 70:200–212.

Sunada, Y., and K. P. Campbell. 1995. Dystrophin-glycoprotein complex: molecular organization and critical roles in skeletal muscle. *Curr. Opin. Neurol.* 8:379–384.

Tidball, J. G., T. O'Halloran, and K. Burridge. 1986. Talin at myotendinous junctions. *J. Cell Biol.* 103:1465–1472.

Tokuyasu, K. T., A. H. Dutton, and S. J. Singer. 1983. Immunoelectron microscopic studies of desmin (skeletin) localization and intermediate filament organization in chicken skeletal muscle. *J. Cell Biol.* 96:1727–1735.

Wang, K., R. McCarter, J. Wright, J. Beverly, and R. Ramirez-Mitchell. 1993. Viscoelasticity of the sarcomere matrix of skeletal muscles. The titin-myosin composite filament is a dual-stage molecular spring. *Biophys. J.* 64:1161–1177.

Wang, K., and R. Ramirez-Mitchell. 1983. A network of transverse and longitudinal intermediate filaments is associated with sarcomeres of adult vertebrate skeletal muscle. *J. Cell Biol.* 96:562–570.

Wang, X., J. Willingale-Theune, R. L. Shoeman, G. Giese, and P. Traub. 1989. Untrastructural analysis of cytoplasmic intermediate filaments and the nuclear lamina in the mouse plasmacytoma cell line MPC-11 after the induction of vimentin synthesis. *Eur. J. Cell Biol.* 50:462–474.

Woodcock, C. L. 1980. Nucleus-associated intermediate filaments from chicken erythrocytes. *J. Cell Biol.* 85:881–889.